

Theory of rare-earth Kramers magnets on a Shastry-Sutherland lattice: dimer phases in the presence of strong spin-orbit coupling

Changle Liu,¹ Guijing Duan,² and Rong Yu^{2,3,*}

¹*School of Engineering, Dali University, Dali, Yunnan 671003, China*

²*School of Physics and Beijing Key Laboratory of Opto-electronic Functional Materials & Micro-nano Devices, Renmin University of China, Beijing 100872, China*

³*Key Laboratory of Quantum State Construction and Manipulation (Ministry of Education), Renmin University of China, Beijing, 100872, China*

(Dated: December 20, 2024)

Shastry-Sutherland magnet is a typical frustrated spin system particularly known for the exact solvability of the singlet dimer phase as well as nearly flat triplon excitations in the Heisenberg limit, while the situation in the presence of strong spin-orbit coupling is not well explored. Motivated by the recently discovered rare-earth Shastry-Sutherland magnets, we derive a generic effective-spin model that describes the interactions between Kramers doublet local moments on a Shastry-Sutherland lattice. Because of the strong spin-orbit coupling, the effective model turns out to be an extended XYZ model on both intra- and inter-dimer bonds. We focus on the dimer phase and show that, in addition to the conventional “singlet” dimer phase in the Heisenberg limit, peculiar “triplet” dimer phases can be stabilized by the strong spin-orbit coupling. While the “singlet” dimer phase, at certain conditions, could still exhibit exact solvability and nearly flat excitations analogous to that in the isotropic Heisenberg model, these “triplet” dimer phases are generally not exactly solvable and exhibit stronger dispersive excitations. We further discuss the thermodynamical and spectral signatures of these “triplet” dimer phases that can be experimentally probed, and illustrate that the recently discovered Shastry-Sutherland magnet $\text{Yb}_2\text{Be}_2\text{GeO}_7$ hosts a triplet dimer ground state.

I. INTRODUCTION

In recent decades, quantum magnetism on the Shastry-Sutherland (SS) lattice has attracted significant attention due to its simple lattice structure yet resultant rich physical behaviors [1–9]. As one of the simplest geometrically frustrated systems in two spatial dimension, the SS model, the $S = 1/2$ Heisenberg antiferromagnetic model defined on the SS lattice, was initially proposed because of the exact solvability of its dimer singlet ground state within certain parameter regime [1, 3]. Meanwhile, this dimer state also exhibits highly localized triplet excitations, and is responsible for the emergence of various plateau phases under an external magnetic field [10–16]. The strong geometrical frustration of the SS model is also clearly manifested in its condensed matter realization, $\text{SrCu}_2(\text{BO}_3)_2$ [2, 4, 7–9, 15–19]. In this compound, the competition between the inter- and intra-dimer interactions, J and J' , leads to a dimerized ground state at ambient pressure. Nearly flat-band excitations have been observed in inelastic neutron scattering [20, 21], and various plateau phases are reported in the in-field phase diagram, all of which support the stabilization of the dimer singlet ground state as predicted in theory. Moreover, when applying a hydrostatic pressure, the ratio between the inter- and intra-dimer couplings J/J' increases, and the ground state evolves to the plaquette and Néel antiferromagnetic (AFM) phases subsequently [7, 11, 18, 22]. The transition from the plaquette to the AFM phase is theoretically proposed to be associated with deconfined quantum criticality, and has attracted much experimental and numerical interest in recent years [8, 11, 22–26].

More recently, research on quantum magnets have been extended to systems with strong spin-orbit coupling (SOC), pushing the boundaries of condensed matter. The strong SOC can give rise to highly anisotropic interactions that frustrates local moments, resulting in highly correlated states with lack of long-range order known as quantum spin liquids (QSL) [27–30], characterized by properties such as fractionalized excitations, emergent gauge structures, and long-range quantum entanglement. Driven by such possibilities, there have been intense experimental and theoretical explorations in the past decade on relevant systems such as honeycomb Kitaev systems [31–38], pyrochlore spin ice [39–41], and large classes of triangular lattice materials [42–51]. Moreover, the interplay between strong SOC and the surrounding crystalline electric field (CEF) environment can give rise to complex forms of multipolar ordering. Aside from magnetic insulators, the multipolar orders have intimate connections to heavy fermion systems, and are responsible for exotic phenomena such as non-Fermi liquid behaviors, unconventional superconductivity, and intricate magnetic or electric responses therein.

Currently, there have been explodingly increasing reports on discoveries of rare-earth SS materials [52–62]. For these systems, two basic questions related to SOC naturally arises: The first one is whether the conclusions holding for the Heisenberg system, such as the exact solvability and highly localized triplet excitations of the dimer phase, would be still valid in the presence of strong SOC. The second one is whether exotic phases or phenomena could be stabilized in the phase diagram by introducing the SOC. Addressing the above questions requires collective efforts from both experiment and theory. On the theory side, it is highly appreciated if we can have understanding on microscopic details of relevant materials, including the structure of local moments as well as

* rong.yu@ruc.edu.cn

the interactions among them. Such knowledge, bridging the theoretical models and experimental observables, would be particularly helpful in analyzing the experimental behaviors of relevant systems.

In a parallel work, Ref. [61], we have developed a theory for rare-earth SS magnets with non-Kramers ions. In this paper we turn to the Kramers counterpart. In contrast to non-Kramers systems where the local moments comprise both magnetic dipoles and quadrupoles, for Kramers systems all the effective-spin components are magnetic dipoles, with the dipole axes that differ in different sublattices. Taking into account the spatial and spin symmetries of this system, we show that the interactions between local moments can be described by an extended XYZ model on both intra- and inter-dimer bonds. Because of the spin anisotropy of this model, the ground state phase diagram contains various dimerized phases, and the exact solvability and nearly-localized triplet excitations within certain regime of the phase diagram that adiabatically connects to the dimer singlet state in the Heisenberg case. Interestingly, we find that several new “triplet” dimer phases can be stabilized with sufficiently strong exchange anisotropy. Such triplet dimer phases are symmetry inequivalent to the singlet one. Moreover, they exhibit various distinct physical behaviors with thermodynamical and spectral signatures that can be directly detected by experiments.

The rest part of the paper is organized as follows. In Sec. II, we analyze the single-ion magnetism and derive the effective Hamiltonian from symmetry analysis. We also analyze the Zeeman coupling of local moments to the external magnetic field that is complicated by the site-dependent local moment structure. In Sec. III we focus on the dimer phase, and show that in addition to the conventional “singlet” dimer phase that appears near the Heisenberg limit, some peculiar “triplet” dimer phases can be stabilized by strong spin-orbit coupling. We compare the “singlet” and “triplet” dimer phases in terms of exact solvability, quantum excitations and their physical behaviors in presence of external magnetic field. Finally, in Sec. IV we summarize and discuss relevance of our results to the Kramers SS magnets [53–55, 58, 59]. In particular, we show that the recently discovered Shastry-Sutherland magnet $\text{Yb}_2\text{Be}_2\text{GeO}_7$ hosts a triplet dimer ground state.

II. EFFECTIVE MODEL

A. Single-ion magnetism

To be concrete, we consider the crystal structure of a class of SS magnets, $\text{RE}_2\text{Be}_2\text{XO}_7$, where $X=\text{Si, Ge, and RE}^{3+}$ ($\text{RE}=\text{Yb, Er, Dy, etc.}$) are rare-earth Kramers ions that form a perfect SS lattice [54, 59]. Without loss of generality, here we take the $\text{Yb}_2\text{Be}_2\text{GeO}_7$ compound [60] with $\text{RE}=\text{Yb}$ as an example, and general results are applicable to all Kramers ions other than Gd^{3+} (given that Gd^{3+} does not carry orbital angular momentum and hence does not have strong SOC). The crystal field scheme of Yb^{3+} is shown in Fig. 1. The magnetism of Yb^{3+} ion is contributed by the partially-filled

electrons within the $4f$ shell. Each Yb^{3+} ion carries orbital angular momentum $L = 3$ and spin angular momentum $S = 1/2$. The strong atomic spin-orbit coupling entangles the spin and orbital degrees of freedom, leading to a total angular momentum $\mathcal{J} = 7/2$ at low energies. The eight-fold $\mathcal{J} = 7/2$ electronic levels are further lifted by the CEF, and split into a series of Kramers doublets protected by time-reversal symmetry. When the temperature is lower than the crystal field splitting between different Kramers doublets, the magnetism is dominated by the lowest Kramers doublet.

The structure of the Kramers local moments can be analyzed from symmetries of the crystal field levels. We define the z direction to be perpendicular to the plane of local moments, and x' and y' are along the two orthogonal dimer directions (see Fig. 2(a)). As the four RE^{3+} sublattices within the unit cell (labeled by RE_i , $i = 0, 1, 2, 3$ as shown in Fig. 2(a)) are connected by the four-fold roto-inversion operation S_4 about the z -axis located at the cell center, we start with the RE_1 sublattice, and the crystal fields of the other three sites are related by the corresponding symmetry operations. Note that the point group symmetry of each RE^{3+} ion only contains a mirror reflection σ_v with the mirror plane parallel to the corresponding dimer direction (mirror planes are indicated by pink solid lines in Fig. 2(a)). For the RE_1 sublattice, we denote the lowest Kramers doublet as $|\psi_{\pm}\rangle$. Since the Kramers ion has a half-integer total angular momentum, its transformation under the crystalline symmetries are quite different from the non-Kramers counterpart. In particular, the eigenvalues of the mirror reflection σ_v become pure imaginary $\pm i$. Denoting $|\psi_{\pm}\rangle$ for the eigenstates of the mirror reflection symmetry, *e.g.*, $\sigma_v|\psi_{\pm}\rangle = \pm i|\psi_{\pm}\rangle$, we can construct an effective spin-1/2 operators by acting the Pauli matrices τ^{α} onto the Kramers doublet: $\hat{\sigma}^{\alpha} \equiv \frac{1}{2} \sum_{\mu\nu} |\psi_{\mu}\rangle \tau_{\mu\nu}^{\alpha} \langle\psi_{\nu}| = \frac{1}{2} \psi \tau^{\alpha} \psi^{\dagger}$ where $\psi = (|\psi_{+}\rangle, |\psi_{-}\rangle)$ and $\alpha = 1, 2, 3$. The symmetry transformations of effective spin components under the mirror reflection σ_v and time-reversal Θ are as follows:

$$\sigma_v : \hat{\sigma}^1 \rightarrow -\hat{\sigma}^1, \hat{\sigma}^2 \rightarrow -\hat{\sigma}^2, \hat{\sigma}^3 \rightarrow \hat{\sigma}^3,$$

$$\Theta : \hat{\sigma}^1 \rightarrow -\hat{\sigma}^1, \hat{\sigma}^2 \rightarrow -\hat{\sigma}^2, \hat{\sigma}^3 \rightarrow -\hat{\sigma}^3.$$

As shown in the above relation, all the three effective spin components are odd under the time-reversal and are thus magnetic dipoles. Moreover, both $\hat{\sigma}^1$ and $\hat{\sigma}^2$ are odd under the mirror reflection σ_v . Hence the corresponding dipole moments lie within the $x'z$ mirror plane (transform as $\mathcal{J}^{x'}$ or \mathcal{J}^z under crystalline symmetries), with specific angles θ_1 and θ_2 , respectively, to the crystal plane. Meanwhile, $\hat{\sigma}^3$ is even under σ_v that transforms as $\mathcal{J}^{y'}$, hence its moment direction is perpendicular to the mirror plane, as illustrated in Fig. 2(b). More quantitatively, the dipolar character of local moments discussed above can be clearly manifested by projecting the total angular momentum \mathcal{J} onto the two-level subspace:

$$\begin{aligned} \hat{\mathbf{j}} &\equiv \mathcal{P}\mathcal{J}\mathcal{P} \\ &= A^{(1)}\hat{\sigma}^1 \mathbf{n}^{(1)} + A^{(2)}\hat{\sigma}^2 \mathbf{n}^{(2)} + A^{(3)}\hat{\sigma}^3 \mathbf{n}^{(3)}, \end{aligned} \quad (1)$$

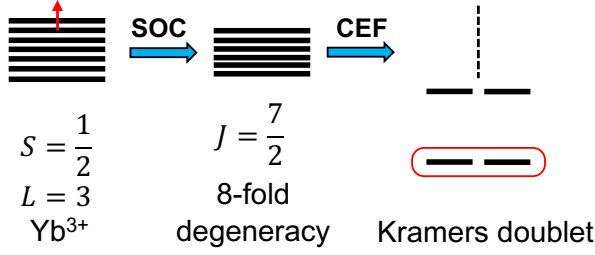


FIG. 1. Crystal field scheme of Yb^{3+} in the rare-earth SS magnet $\text{Yb}_2\text{Be}_2\text{GeO}_7$. The red arrow represents one hole in the $4f$ shell. Under strong SOC and CEF the electronic levels split into a set of Kramers doublets. At low temperatures, the magnetism is dominated by the lowest Kramers doublet which is well separated to other Kramers doublets.

where $\mathcal{P} \equiv \psi\psi^\dagger = |\psi_+\rangle\langle\psi_+| + |\psi_-\rangle\langle\psi_-|$ is the projection operator onto the lowest doublet subspace, $A^{(\alpha)}$ describes the magnitude of the dipole moment $\hat{\sigma}^\alpha$, and $\mathbf{n}^{(\alpha)}$ are unit vectors representing the directions of dipoles $\hat{\sigma}^\alpha$ ($\alpha = 1, 2, 3$). Note that $\mathbf{n}^{(3)}$ is completely fixed by symmetries to be perpendicular to the mirror plane. However, the symmetry cannot fully determine the directions of $\mathbf{n}^{(1)}$ and $\mathbf{n}^{(2)}$: They are constrained to lie within the mirror plane, but their precise directions must be determined by the exact wave functions of the crystal fields. As a consequence, the dipole axes are in general non-orthogonal, *i.e.*, $\mathbf{n}^{(1)} \cdot \mathbf{n}^{(2)} \neq 0$, due to the low point group symmetries of the rare-earth sites.

The above discussions are restricted to the RE_1 ion. As the four RE_i sublattices within the unit cell are connected by the four-fold roto-inversion S_4 , the directions of dipoles at different sites $\mathbf{n}_i^{(\alpha)}$ are connected by the corresponding four-fold counter-rotation about the z axis. Therefore, for different sublattices, $\mathbf{n}_i^{(1)}$ and $\mathbf{n}_i^{(2)}$ must have the same out-of-plane component, while the directions of in-plane components are illustrated by the blue arrows in Fig. 2(a). Meanwhile, $\mathbf{n}_i^{(3)}$ are located within the crystal plane with directions as shown by the red arrows in Fig. 2(a).

B. Effective Hamiltonian

Here we derive a generic effective Hamiltonian based on symmetry analysis. Due to the strongly localized nature of the $4f$ electrons, it is sufficient to consider only the intra-dimer and the nearest-neighbor (NN) inter-dimer interactions.

We begin with the intra-dimer interaction. For each dimer bond, there exist two mirror symmetries σ_v and σ'_v , with the mirror planes located parallel and perpendicular to the bond directions, respectively. Suppose the generic intra-dimer interactions are of the following bilinear form: $H_J = \sum_{\langle\langle ij \rangle\rangle\alpha\beta} J_{ij}^{\alpha\beta} \hat{\sigma}_i^\alpha \hat{\sigma}_j^\beta$. Since $\hat{\sigma}^3$ has different parity from $\hat{\sigma}^1$ and $\hat{\sigma}^2$ under the σ_v , they are not allowed to mix linearly: $J_{ij}^{\prime 13} = J_{ij}^{\prime 23} = J_{ij}^{\prime 31} = J_{ij}^{\prime 32} = 0$. Moreover, the σ'_v mirror reflection exchanges the positions of two sites. This guarantees $J_{ij}^{\prime 12} =$

$J_{ji}^{\prime 21}$. As a consequence, the antisymmetric Dzyaloshinskii-Moriya (DM) interaction [63, 64] is disallowed, and the intra-dimer interaction simply takes the form

$$H_J = \sum_{\langle\langle ij \rangle\rangle} (\hat{\sigma}_i^1, \hat{\sigma}_i^2, \hat{\sigma}_i^3) \begin{pmatrix} J^{\prime 11} & J^{\prime 12} \\ J^{\prime 12} & J^{\prime 22} \\ J^{\prime 33} & \end{pmatrix} \begin{pmatrix} \hat{\sigma}_j^1 \\ \hat{\sigma}_j^2 \\ \hat{\sigma}_j^3 \end{pmatrix}.$$

The form of interaction can be further simplified if we perform a global basis rotation on the CEF basis $|\psi_\pm\rangle$ at each site, so that the cross-coupling term $J^{\prime 12}$ can be eliminated. The resulting interaction is an XYZ model similar to the case of non-Kramers systems [61]

$$H_J = \sum_{\langle\langle ij \rangle\rangle} J^{\prime 11} \hat{\sigma}_i^1 \hat{\sigma}_j^1 + J^{\prime 22} \hat{\sigma}_i^2 \hat{\sigma}_j^2 + J^{\prime 33} \hat{\sigma}_i^3 \hat{\sigma}_j^3. \quad (2)$$

Note that although this system lacks inversion symmetry about the bond center, intra-dimer DM interaction is still not allowed by crystalline symmetries. This is because that our local moments, which are subjected to strong SOC, transform differently under crystalline symmetries compared to pure spins. This issue will be discussed in more detail in Sec. IV.

Then we consider the NN inter-dimer interaction that takes the generic form $H_J = \sum_{\langle\langle ij \rangle\rangle\alpha\beta} J_{ij}^{\alpha\beta} \hat{\sigma}_i^\alpha \hat{\sigma}_j^\beta$. Since there is no symmetries to constrain the interaction within each bond, the NN inter-dimer interaction take the form

$$H_J = \sum_{\langle\langle ij \rangle\rangle} (\hat{\sigma}_i^1, \hat{\sigma}_i^2, \hat{\sigma}_i^3) \begin{pmatrix} J^{11} & J^{12} & \eta_{ij} J^{13} \\ J^{21} & J^{22} & \eta_{ij} J^{23} \\ \eta_{ij} J^{31} & \eta_{ij} J^{32} & J^{33} \end{pmatrix} \begin{pmatrix} \hat{\sigma}_j^1 \\ \hat{\sigma}_j^2 \\ \hat{\sigma}_j^3 \end{pmatrix} \\ \equiv \sum_{\langle\langle ij \rangle\rangle} \hat{\sigma}_i \cdot \mathbf{J}_{ij} \cdot \hat{\sigma}_j. \quad (3)$$

Here $\hat{\sigma}_i = (\hat{\sigma}_i^1, \hat{\sigma}_i^2, \hat{\sigma}_i^3)^T$, \mathbf{J}_{ij} denotes the interaction matrices of the $\langle\langle ij \rangle\rangle$ bond, $\langle\langle ij \rangle\rangle$ follows the bond direction $i \rightarrow j$ as shown in Fig. 2(c), and η_{ij} takes the value ± 1 for the red and blue bonds as in Fig. 2(c), respectively. Note that for the NN inter-dimer interaction, the DM interaction is allowed by symmetry. Moreover, there can be two types of DM interactions: the bond-independent one $H_{DM}^{(1)} = \sum_{\langle\langle ij \rangle\rangle} \mathbf{D}^{(1)} \cdot (\hat{\sigma}_i \times \hat{\sigma}_j)$ and the bond-dependent one $H_{DM}^{(2)} = \sum_{\langle\langle ij \rangle\rangle} \mathbf{D}_{ij}^{(2)} \cdot (\hat{\sigma}_i \times \hat{\sigma}_j)$, with $\mathbf{D}^{(1)} = (0, 0, D^z)$ and $\mathbf{D}_{ij}^{(2)} = \eta_{ij}(D^x, D^y, 0)$. Both types of the DM interactions respect the crystalline four-fold S_4 symmetry of the system.

Unlike the non-Kramers systems, the crystal field levels of Kramers systems are pair-degenerate as protected by the time-reversal symmetry, indicating that no intrinsic field term is present. So the total Hamiltonian takes the form

$$H = H_J + H_J'. \quad (4)$$

C. Coupling to magnetic field

For Kramers systems, all the three spin components are magnetic dipoles that directly couple to the external magnetic

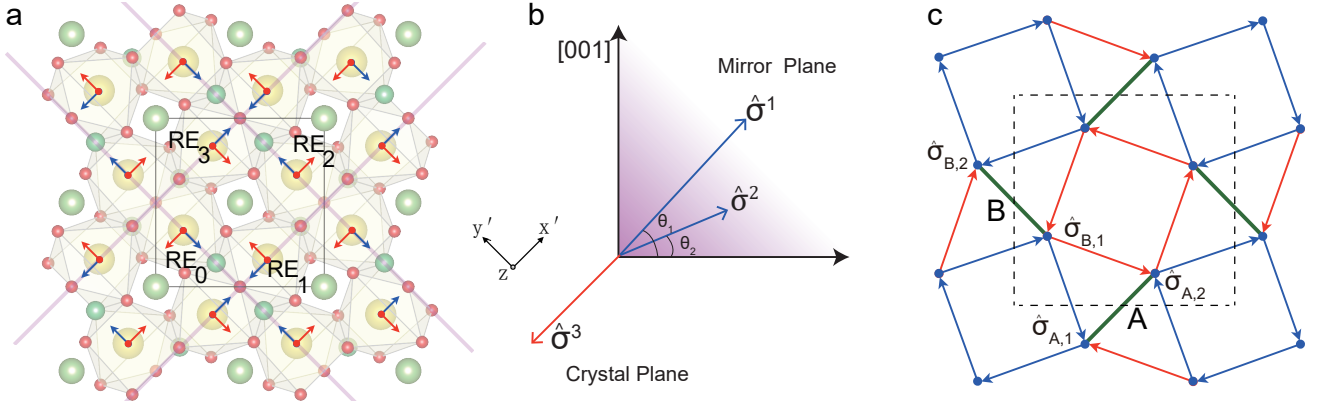


FIG. 2. **Crystal structure and dipole axes of SS magnets with Kramers local moments.** **a** Crystal structure of $\text{Yb}_2\text{Be}_2\text{GeO}_7$. Yb^{3+} and O^{2-} are denoted by yellow and red balls, respectively. Mirror planes of Yb^{3+} are denoted by purple lines. The in-plane directions of $\hat{\sigma}^1$ and $\hat{\sigma}^2$ dipole axes are denoted by the blue arrows, while that of $\hat{\sigma}^3$ is indicated by the red arrows. **b** Illustration of dipole axes. The $\hat{\sigma}^1$ and $\hat{\sigma}^2$ components are within the mirror plane, while the $\hat{\sigma}^3$ component is perpendicular to the mirror plane. $\hat{\sigma}^1$ and $\hat{\sigma}^2$ are generally non-orthogonal. **c** Illustration of the SS lattice. Each unit cell contains two dimer bonds denoted by the thick dark green lines and marked by A, B, respectively. The NN inter-dimer bonds can also be divided into two groups, characterized by $\eta_{ij} = \pm 1$ in Eq. (3), and are marked red and blue, respectively, with the directions $i \rightarrow j$ indicated by arrows.

field. As the dipole axes of different sites only depend on their sublattices indices, for simplicity here we only consider four rare-earth sites within a unit cell, where each sites are labeled by their sublattice indices i ($i = 0, 1, 2, 3$). The general form of the Zeeman coupling takes the form

$$H_{\text{Zeeman}} = - \sum_{i=0}^3 \mu_B \mathbf{B} \cdot \mathbf{g}_i \cdot \hat{\sigma}_i, \quad (5)$$

where $(\mathbf{g}_i)_{\alpha\beta} = g_J A^{(\beta)} n_{i,\alpha}^{(\beta)}$ is the g -tensor for the effective spins. Due to the site-dependence of the local dipole axes $\mathbf{n}_i^{(\alpha)}$, the external magnetic field couple to the effective spins in some complicated manner as follows

$$H_{[001]} = -\mu_B g_J B^{[001]} \sum_{i=0}^3 \left(A_{\perp}^{(1)} \hat{\sigma}_i^1 + A_{\perp}^{(2)} \hat{\sigma}_i^2 \right), \quad (6)$$

$$H_{[110]} = -\mu_B g_J B^{[110]} \times \left[A_{\parallel}^{(1)} (\hat{\sigma}_3^1 - \hat{\sigma}_1^1) + A_{\parallel}^{(2)} (\hat{\sigma}_3^2 - \hat{\sigma}_1^2) + A^{(3)} (\hat{\sigma}_2^3 - \hat{\sigma}_0^3) \right], \quad (7)$$

$$H_{[\bar{1}10]} = -\mu_B g_J B^{[\bar{1}10]} \times \left[A_{\parallel}^{(1)} (\hat{\sigma}_2^1 - \hat{\sigma}_0^1) + A_{\parallel}^{(2)} (\hat{\sigma}_2^2 - \hat{\sigma}_0^2) + A^{(3)} (\hat{\sigma}_1^3 - \hat{\sigma}_3^3) \right], \quad (8)$$

where $A_{\parallel}^{(\alpha)} \equiv A_{\parallel}^{(\alpha)} \cos \theta_{\alpha}$ and $A_{\perp}^{(\alpha)} \equiv A_{\perp}^{(\alpha)} \sin \theta_{\alpha}$ correspond to the magnitudes of the in-plane and out-of-plane components of the dipole moments $\hat{\sigma}^{\alpha}$ ($\alpha = 1, 2$), respectively. As shown above, the out-of-plane and in-plane magnetic fields couple to the uniform and staggered dipolar magnetization, respectively. The different ways of coupling will have

profound implications in the magnetization process of the “singlet” and “triplet” dimer phases, as will be discussed in the next section. Meanwhile, as the external magnetic field always couple to multiple components of effective spins, the high temperature magnetic susceptibilities would generally exhibit non-Curie-Weiss behaviors. As such non-Curie-Weiss behaviors are difficult to analyze in experiments, we will not discuss them in detail here in our present work.

III. DIMER PHASES IN THE PRESENCE OF STRONG SOC

To reveal physical effects of the strong SOC, we focus on the dimer phase where intra-dimer interactions dominate over the inter-dimer ones. For the isotropic (Heisenberg) SS model, the dimer phase is particularly notable for its exact solvability: the product state of dimer singlets is the exact ground state of the system when $J/J' \lesssim 0.675$ [22, 23]. As the quantum entanglement of this state is restricted within each dimer, the low-lying quantum excitations must be highly localized. Indeed, the single triplet excitations are nearly flat, with very weak dispersion caused by the sixth and higher order terms in J/J' [2, 65, 66]. In the following we will show that under certain limits, the above conclusions for the isotropic Heisenberg systems still hold in the presence of the XYZ anisotropy.

We first consider the strong intra-dimer limit where the inter-dimer interactions are neglected, so that the ground state becomes a product state of decoupled dimers. Due to the presence of XYZ anisotropy, the four eigenstates within each dimer are in general non-degenerate, which are labeled as

$$|s\rangle = \frac{1}{\sqrt{2}} (|\uparrow\downarrow\rangle - |\downarrow\uparrow\rangle), \quad (9)$$

$$|t_1\rangle = \frac{-1}{\sqrt{2}} (|\uparrow\uparrow\rangle - |\downarrow\downarrow\rangle), \quad (10)$$

$$|t_2\rangle = \frac{i}{\sqrt{2}} (|\uparrow\uparrow\rangle + |\downarrow\downarrow\rangle), \quad (11)$$

$$|t_3\rangle = \frac{1}{\sqrt{2}} (|\uparrow\downarrow\rangle + |\downarrow\uparrow\rangle), \quad (12)$$

with energies $\epsilon_s = -(J^{11} + J^{22} + J^{33})/4$ and $\epsilon_{t_\alpha} = -\epsilon_s - J^{\alpha\alpha}/2$ ($\alpha = 1, 2, 3$). Note that here $|t_\alpha\rangle$ is chosen as the eigenstate of the total spin operator $\hat{T}^\alpha \equiv \hat{\sigma}_1^\alpha + \hat{\sigma}_2^\alpha$: $\hat{T}^\alpha |t_\alpha\rangle = 0$. Following the convention of isotropic Heisenberg dimers, here we still denote $|s\rangle$ as ‘‘singlet’’ dimer and $|t_\alpha\rangle$ as ‘‘triplet’’ dimers respectively, despite that all the energy levels are no longer degenerate.

The phase diagram in the intra-dimer limit is shown in Fig. 3. Depending on the values of $J^{\alpha\alpha}$, any of the four dimer states can be the ground state of the system. Hence we can have four types of dimer ground states described by the product state of $|s\rangle$ and/or $|t_\alpha\rangle$ on each dimer, respectively. The fact that ‘‘triplet’’ dimer states are physically distinct from the singlet ones can be derived from symmetries. In fact, for each dimer, the singlet and triplet states transform differently under spatial symmetries

$$\sigma_v : |s\rangle \rightarrow +|s\rangle, |t_1\rangle \rightarrow -|t_1\rangle, |t_2\rangle \rightarrow -|t_2\rangle, |t_3\rangle \rightarrow +|t_3\rangle,$$

$$\sigma'_v : |s\rangle \rightarrow -|s\rangle, |t_1\rangle \rightarrow -|t_1\rangle, |t_2\rangle \rightarrow -|t_2\rangle, |t_3\rangle \rightarrow +|t_3\rangle.$$

The different symmetry representations of singlet and triplet states forbids their mutual mixing as long as the crystalline symmetries are preserved. Therefore, singlet and triplet dimer phases remain symmetry distinct phases even when the inter-dimer interactions H_J is introduced. Also note that $|t_1\rangle$ and $|t_2\rangle$ triplet states share the same symmetry representation and this is because the effective-spin components $\hat{\sigma}^1$ and $\hat{\sigma}^2$ transform in the same way under spatial symmetries.

The inter-dimer interaction H_J introduces correlated quantum tunneling process of nearby dimers. Such quantum fluctuations can be quantitatively described within the bond-operator formalism [67–69]. In this formalism, each dimer state $|s\rangle$ or $|t_\alpha\rangle$ can be expressed by creating a bond-operator boson out of the vacuum $|\text{vac}\rangle$, *i.e.*,

$$|s\rangle = \hat{s}^\dagger |\text{vac}\rangle, |t_\alpha\rangle = \hat{t}_\alpha^\dagger |\text{vac}\rangle.$$

The Hilbert space of the bosons is larger than the original dimer Hilbert space and includes unphysical states. To limit the boson Hilbert space to its physical sector, a hard-core constraint must be imposed on each dimer,

$$\hat{s}^\dagger \hat{s} + \sum_\alpha \hat{t}_\alpha^\dagger \hat{t}_\alpha = 1. \quad (13)$$

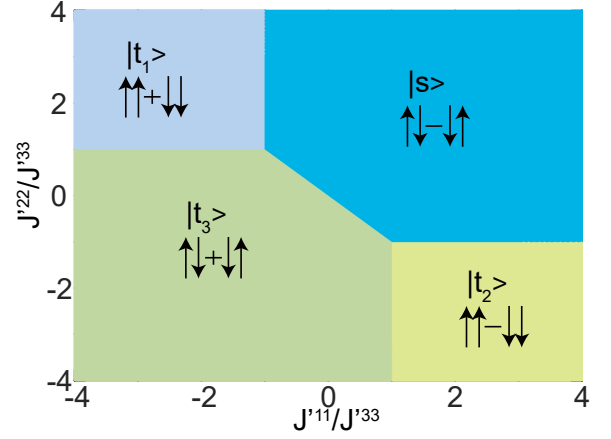


FIG. 3. Phase diagram of the effective model Eq. (4) in the intra-dimer limit $J_{ij} = 0$. Here J^{33} is set antiferromagnetic.

The two spins within a dimer can be expressed as quadratics of bond operators,

$$\hat{\sigma}_1^\alpha = +\frac{1}{2} (\hat{s}^\dagger \hat{t}_\alpha + \hat{t}_\alpha^\dagger \hat{s}) - \frac{i}{2} \epsilon_{\alpha\beta\gamma} \hat{t}_\beta^\dagger \hat{t}_\gamma, \quad (14)$$

$$\hat{\sigma}_2^\alpha = -\frac{1}{2} (\hat{s}^\dagger \hat{t}_\alpha + \hat{t}_\alpha^\dagger \hat{s}) - \frac{i}{2} \epsilon_{\alpha\beta\gamma} \hat{t}_\beta^\dagger \hat{t}_\gamma, \quad (15)$$

for $\alpha, \beta, \gamma = 1, 2, 3$. Note that for each dimer, the total spin \hat{T}^α can be expressed as

$$\hat{T}^\alpha \equiv \hat{\sigma}_1^\alpha + \hat{\sigma}_2^\alpha = -i \epsilon_{\alpha\beta\gamma} \hat{t}_\beta^\dagger \hat{t}_\gamma, \quad (16)$$

that only involves hopping between triplets but not singlet. Meanwhile, a single spin operator $\hat{\sigma}_{1,2}^\alpha$ involves both triplet hopping process, as well as mixing between singlet and triplets.

Note that the above discussions are limited to a single dimer. In the SS lattice, each unit cell contains two dimers, so each dimer can be uniquely labeled by its unit cell position \mathbf{r} and the dimer index $\delta = A, B$, as shown in Fig. 2(c). The intra-dimer interaction H_J is diagonal in the bond-operator representation that can be recast as the chemical potential of bosons

$$H_J = \sum_{\mathbf{r}, \delta=A, B} \left(\epsilon_s \hat{s}_{\mathbf{r}, \delta}^\dagger \hat{s}_{\mathbf{r}, \delta} + \sum_\alpha \epsilon_{t_\alpha} \hat{t}_{\mathbf{r}, \delta, \alpha}^\dagger \hat{t}_{\mathbf{r}, \delta, \alpha} \right), \quad (17)$$

while the inter-dimer H_J term provides off-diagonal quantum dynamics to the system. In the following, we will discuss the quantum dynamical behaviors of the singlet and triplet dimer phases separately.

A. The ‘‘Singlet’’ dimer $|s\rangle$ phase

As has been discussed previously, the ‘‘singlet’’ dimer state, corresponding to the product state of singlet $|s\rangle$ within each

dimer $|\psi_s\rangle \equiv \prod_{\mathbf{r}} \hat{s}_{\mathbf{r},A}^\dagger \hat{s}_{\mathbf{r},B}^\dagger |\text{vac}\rangle$, has been proved to be the exact eigenstate of the isotropic Heisenberg SS model in all parameter regime, and becomes the exact ground state when $J/J' \lesssim 0.675$. For the anisotropic XYZ model we considered here, the ‘‘singlet’’ state $|s\rangle$ remains to be the ground state provided $J^{\alpha\alpha} + J^{\beta\beta} > 0$ for all $\alpha, \beta = 1, 2, 3$. Therefore, the ‘‘singlet’’ dimer state can be stable even in the presence of significant XYZ anisotropy.

To reveal its quantum dynamics, we first consider a simple limit $J^{13} = J^{23} = J^{31} = J^{32} = 0$, making the interactions of the red and blue bond identical, *i.e.*, $J_{ij} = J$. Note that in this case the anti-symmetric DM interaction $H_{DM}^{(1)} = \sum_{\langle ij \rangle} \mathbf{D}^{(1)} \cdot (\hat{\sigma}_i \times \hat{\sigma}_j)$ as well the symmetric interaction $H_\Gamma = \sum_{\langle ij \rangle} \Gamma (\hat{\sigma}_i^1 \hat{\sigma}_j^2 + \hat{\sigma}_i^2 \hat{\sigma}_j^1)$ are still allowed. Then, the NN inter-dimer interactions can be recast as interactions of each spin in one dimer with the total spin of its adjacent dimer,

$$H_J = \sum_{\mathbf{r}} [\hat{\sigma}_{\mathbf{r},B,1} \cdot \mathbf{J} \cdot \hat{\mathbf{T}}_{\mathbf{r},A} + \hat{\sigma}_{\mathbf{r},A,2} \cdot \mathbf{J} \cdot \hat{\mathbf{T}}_{\mathbf{r}+\mathbf{a},B} + \hat{\sigma}_{\mathbf{r}+\mathbf{a},B,2} \cdot \mathbf{J} \cdot \hat{\mathbf{T}}_{\mathbf{r}+\mathbf{b},A} + \sigma_{\mathbf{r}+\mathbf{b},A,1} \cdot \mathbf{J} \cdot \hat{\mathbf{T}}_{\mathbf{r},B}]. \quad (18)$$

Note that the total spin operator $\hat{\mathbf{T}}$ only involves bilinears of triplet operators, it vanishes when acting upon the singlet dimer state: $\hat{\mathbf{T}}_{\mathbf{r}} |\psi_s\rangle = 0$. Therefore, we have

$$H_J |\psi_s\rangle = 0, \quad (19)$$

the singlet dimer state $|\psi_s\rangle$ remains to be an exact eigenstate even in the presence of XYZ anisotropy.

The excitations above the singlet dimerized state can be obtained by condensing the singlet boson where a single boson \hat{s} gains a non-vanishing expectation value

$$\hat{s} = \hat{s}^\dagger \approx \sqrt{1 - \sum_{\alpha} \hat{t}_{\alpha}^\dagger \hat{t}_{\alpha}}, \quad (20)$$

then the triplet can be regarded as elementary quantum excitations in this dimerized phase. More details about this bond-operator approach is presented in Appendix. By expanding H_J in terms of triplet bosons order-by-order, we find that at the quadratic level no triplet bilinears present, indicating that triplet excitations are almost localized, see Fig. 4(a). By applying perturbation theory, we find that the dispersion of triplet excitations can only be caused by the sixth and higher orders of triplet operators in H_J , analogous to the isotropic Heisenberg case [10, 70, 71].

The above discussions are limited to the case $J^{13} = J^{23} = J^{31} = J^{32} = 0$. Away from this limit, H_J involves second-order of the singlet operators $\sim t^\dagger s t^\dagger s$, as correlated tunneling of two nearby singlet dimers to triplet dimers. On one hand, such correlated tunneling process makes the singlet dimer product state $|\psi_s\rangle$ no longer the exact eigenstate of the system. On the other hand, condensation of singlet bosons results in direct hopping of triplet bosons at the first order of H_J . Therefore, a non-zero J^{13}, J^{23}, J^{31} or J^{32} would contribute to a more considerable bandwidth of single triplet excitations linear in H_J , see Fig. 4(b).

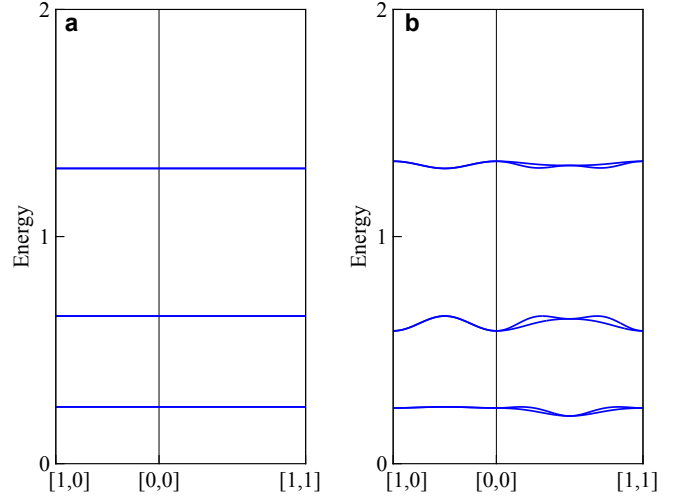


FIG. 4. **Dispersion of excitations in the singlet dimer phase obtained by linear bond-operator theory.** The system parameters taken are $J^{11} = 1.7, J^{22} = 0.9, J^{11} = -0.4, J^{11} = J^{22} = J^{33} = 0.3, J^{12} = 0.1, J^{21} = 0$, **a** $J^{13} = J^{23} = J^{31} = J^{32} = 0$ that results a flat dispersion; **b** $J^{13} = 0.1, J^{23} = 0.13, J^{31} = 0.05, J^{32} = -0.05$ that results dispersive excitations.

B. The ‘‘triplet’’ $|t_\alpha\rangle$ dimer phase

If the ‘‘triplet’’ $|t_\alpha\rangle$ state has the lowest energy within a dimer, the ‘‘triplet’’ dimer state, as described by the variational wave functions of $|t_\alpha\rangle$ triplet product state $|\psi_{t_\alpha}\rangle = \prod_{\mathbf{r}} \hat{t}_{\mathbf{r},A,\alpha}^\dagger \hat{t}_{\mathbf{r},B,\alpha}^\dagger |\text{vac}\rangle$, will be stabilized as the ground state of the system in the $H_J = 0$ limit. Stabilizing such triplet dimer state requires strong spin anisotropy, *i.e.*, it requires that at least one $J^{\alpha\alpha}$ is ferromagnetic and has a larger absolute value than one of the antiferromagnetic $J^{\alpha\alpha}$ values. Similarly, the quantum dynamics of the triplet dimer phase can be investigated by expressing H_J in terms of the bond operators. We find that there exists terms such as $t_\beta^\dagger t_\beta^\dagger t_\alpha t_\alpha$ ($\beta \neq \alpha$) in H_J that drives the system away from the pure product state $|\psi_{t_\alpha}\rangle$. Hence $|\psi_{t_\alpha}\rangle$ is not an exact eigenstate of the system if a finite inter-dimer coupling H_J is present. Meanwhile, the quantum excitations above the triplet dimer state $|\psi_{t_\alpha}\rangle$ can be obtained by condensing \hat{t}_α

$$\hat{t}_\alpha = \hat{t}_\alpha^\dagger \approx \sqrt{1 - \hat{s}^\dagger \hat{s} - \sum_{\beta \neq \alpha} \hat{t}_\beta^\dagger \hat{t}_\beta}. \quad (21)$$

The dispersion of quantum excitation is presented in Fig. 5. We note that in the triplet dimer phase, \hat{t}_β ($\beta \neq \alpha$) excitations are generally dispersive, in sharp contrast to the singlet dimer phase. This is because of the presence of $t_\beta^\dagger t_\beta^\dagger t_\alpha t_\alpha$ terms ($\beta \neq \alpha$) in H_J .

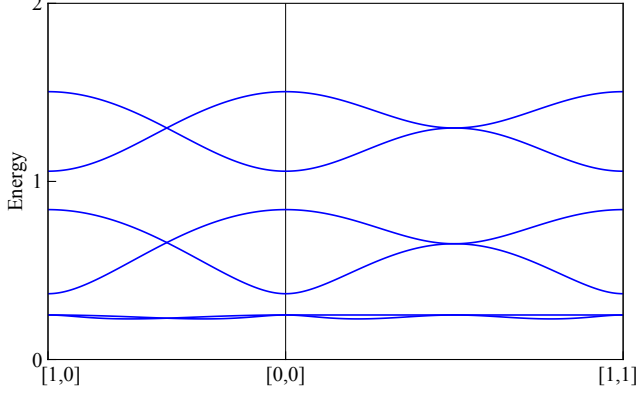


FIG. 5. **Dispersion of excitations in the triplet dimer phase obtained from the linear bond-operator theory.** The system lies within the $|\psi_{t_2}\rangle$ phase with exchange parameters $J^{11} = 1.7$, $J^{22} = -0.9$, $J^{11} = 0.4$, $J^{11} = J^{22} = J^{33} = 0.11$, $J^{12} = 0.07$, $J^{13} = J^{21} = J^{23} = J^{31} = J^{32} = 0$.

C. Stability under small magnetic fields

In this and the following subsections, we discuss the experimental signatures of singlet and triplet dimer phases in the presence of external magnetic fields. To simplify our discussions, we assume that the system lies deep within the dimer phase and the inter-dimer interactions can be ignored compared to the intra-dimer ones. A comparison on distinct experimental behaviors of singlet and triplet dimer phases is summarized in Tab. I.

We first discuss the stability of the singlet and triplet dimer phases under a small external magnetic field. As mentioned previously, in our Kramers systems the coupling to the magnetic field takes complicated forms, with the out-of-plane and in-plane field components coupled to the uniform and staggered dipolar magnetizations, respectively. In the following we will discuss these two cases separately.

Note that within each unit cell there are two dimers denoted by the dimer indices $\delta = A, B$. When an external magnetic field is applied in the out-of-plane [001] direction, each dimer couples to the external field in a uniform way according to Eq. (6). Therefore, it is sufficient to consider only a single dimer, say, the $\delta = B$ dimer formed by RE_0 and RE_2 . The Zeeman coupling along the [001] field direction takes the form

$$H_{[001]} = -\mu_B g_J B^{[001]} \sum_{i=0,2} (A_{\perp}^{(1)} \hat{\sigma}_i^1 + A_{\perp}^{(2)} \hat{\sigma}_i^2), \quad (22)$$

and is represented in the matrix form with the dimer basis $\psi \equiv (|s\rangle |t_1\rangle |t_2\rangle |t_3\rangle)^T$:

$$H_{[001]} = -\mu_B g_J B^{[001]} \begin{pmatrix} 0 & & & \\ & 0 & & iA_{\perp}^{(2)} \\ & & 0 & -iA_{\perp}^{(1)} \\ -iA_{\perp}^{(2)} & iA_{\perp}^{(1)} & & 0 \end{pmatrix}. \quad (23)$$

In the presence of the magnetic field $\parallel [001]$, the three triplet states $|t_{\alpha}\rangle$ will mix with each other. Meanwhile, the singlet state $|s\rangle$ cannot mix with triplet states as is forbidden by symmetries: $H_{[001]}$ is odd under both σ_v and σ'_v ; The mixing between $|s\rangle$ and $|t_3\rangle$ is forbidden by σ'_v , while mixing between $|s\rangle$ and $|t_1\rangle$ ($|t_2\rangle$) is forbidden by σ_v . Therefore, the singlet state $|s\rangle$ remains unaffected as an eigenstate of the dimer system. If the singlet state is the zero-field ground state, it will remain stable within a certain range of magnetic fields, forming an approximate zero magnetization plateau with suppressed magnetic susceptibility at low temperatures. On the other hand, if the zero-field ground state belongs to the triplet dimer states $|\psi_{t_{\alpha}}\rangle$, an infinitesimal field can already induce a non-zero magnetization. Therefore, we expect a pronounced low-temperature magnetic susceptibility for the triplet dimer states.

Then we consider the in-plane magnetic field, say, along the [110] direction. In this case, the two dimers labeled by $\delta = A, B$ couple to the magnetic field differently, so we will discuss them separately. We first consider the $\delta = B$ dimer formed by RE_0 and RE_2 . The Zeeman coupling is

$$H_{[110]}^{(B)} = -\mu_B g_J B^{[110]} A_{\parallel}^{(3)} (\hat{\sigma}_2^3 - \hat{\sigma}_0^3), \quad (24)$$

with the matrix representation in the ψ basis

$$H_{[110]}^{(B)} = \mu_B g_J B^{[110]} \begin{pmatrix} 0 & & A_{\parallel}^{(3)} & \\ & 0 & & \\ & & 0 & \\ A_{\parallel}^{(3)} & & & 0 \end{pmatrix}. \quad (25)$$

In this case, the singlet $|s\rangle$ will mix with $|t_3\rangle$, while $|t_1\rangle$ and $|t_2\rangle$ remain unaffected by the field. Meanwhile, for the $\delta = A$ dimer formed by RE_1 and RE_3 , the matrix representation of the Zeeman coupling takes the form

$$H_{[110]}^{(A)} = -\mu_B g_J B^{[110]} [A_{\parallel}^{(1)} (\hat{\sigma}_3^1 - \hat{\sigma}_1^1) + A_{\parallel}^{(2)} (\hat{\sigma}_3^2 - \hat{\sigma}_1^2)], \quad (26)$$

with the matrix representation

$$H_{[110]}^{(A)} = \mu_B g_J B^{[110]} \begin{pmatrix} 0 & A_{\parallel}^{(1)} & A_{\parallel}^{(2)} & 0 \\ A_{\parallel}^{(1)} & 0 & & \\ A_{\parallel}^{(2)} & & 0 & \\ 0 & & & 0 \end{pmatrix}. \quad (27)$$

Therefore, for the $\delta = A$ dimer, the singlet $|s\rangle$ will mix with $|t_1\rangle$ and $|t_2\rangle$, while $|t_3\rangle$ remain unaffected. Combining the magnetization process of the two dimers, we conclude that

	Singlet dimer phase	Triplet dimer phases
Excitation dispersion	Less dispersive	More dispersive
Zero-magnetization plateau	Present	Absent
M vs B curve	Discontinuous	Continuous and smooth
Zero-field magnetic susceptibility	Suppressed	Pronounced
ΔE vs B curve	Non-analytical with gap closure	Smooth without gap closure

TABLE I. Comparison of experimental signatures for the singlet and triplet dimer phases at low temperatures. Here the magnetic field is applied along to the [001] direction.

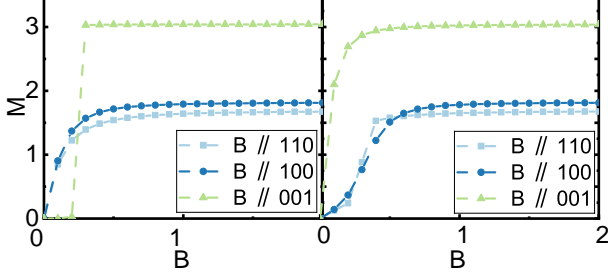


FIG. 6. Magnetization process of dimer phases upon external magnetic fields. **a** singlet dimer phase $|s\rangle$, with parameters $J^{11} = 1.4$, $J^{22} = 1.7$, $J^{33} = 1$. **b** triplet dimer phase $|t_3\rangle$, with parameters $J^{11} = -1.4$, $J^{22} = -1.7$, $J^{33} = 1$. In both cases we set parameters $\mu_B g_J A_{\parallel}^{(1)} = 1.1$, $\mu_B g_J A_{\parallel}^{(2)} = 2.1$, $\mu_B g_J A_{\parallel}^{(3)} = 1.0$, $\mu_B g_J A_{\perp}^{(1)} = 2.2$, $\mu_B g_J A_{\perp}^{(2)} = 2.1$. The temperature is set to $T = 0.1J^{33}$. The calculations are performed using the exact diagonalization of decoupled dimers.

under an in-plane magnetic field, all the dimer states will become unstable and become magnetized by the field, hence the whole system will not exhibit any zero magnetization plateau (Fig. 6).

D. Spectral evolution under magnetic field \parallel [001]

Here we discuss the evolution of excitation spectra under external magnetic fields that can be investigated through neutron scattering, terahertz spectroscopy and electron spin resonance experiments. To simplify our discussions, we consider that the magnetic field is applied along [001] direction, *i.e.*, $\mathbf{B} = B\hat{z}$. We also assume that the system lies deep within the dimer phase and the inter-dimer interactions can be ignored compared to the intra-dimer ones. As previously mentioned, under magnetic fields \parallel [001], the mixing between the singlet and triplet levels are forbidden by symmetries. The energy of the singlet state $|s\rangle$ remains unaffected in the presence of the magnetic field:

$$E_s(B) = \epsilon_s. \quad (28)$$

In contrast, the three triplet states experience mutually mixing in presence of magnetic fields. Such mutual mixing will result avoided level crossing of triplets under magnetic field. However, level crossing between the singlet and triplet levels

still are allowed by symmetries. We denote the three triplet eigenstates as $|t, -\rangle$, $|t, 0\rangle$, $|t, +\rangle$ with energies $E_{t,-}(B) < E_{t,0}(B) < E_{t,+}(B)$. In the limit where the field dominates over the exchange interactions, the energies of the three triplet levels $|t, \pm\rangle$, $|t, 0\rangle$ can be obtained from the non-degenerate perturbation theory:

$$E_{t,\pm}(B) = \pm\mu_B g_J B \sqrt{(A_{\perp}^{(1)})^2 + (A_{\perp}^{(2)})^2} + E_{t,\pm}^{(0)} + O(1/B), \quad (29)$$

$$E_{t,0}(B) = E_{t,0}^{(0)} + O(1/B), \quad (30)$$

where

$$E_{t,\pm}^{(1)} = \frac{1}{2} \left[\frac{(A_{\perp}^{(2)})^2 \epsilon_{t_1} + (A_{\perp}^{(1)})^2 \epsilon_{t_2}}{(A_{\perp}^{(1)})^2 + (A_{\perp}^{(2)})^2} + \epsilon_{t_3} \right], \quad (31)$$

$$E_{t,0}^{(1)} = \frac{(A_{\perp}^{(1)})^2 \epsilon_{t_1} + (A_{\perp}^{(2)})^2 \epsilon_{t_2}}{(A_{\perp}^{(1)})^2 + (A_{\perp}^{(2)})^2} \quad (32)$$

are the first-order perturbations that exhibit no field dependence, and $O(1/B)$ comes from the second-order corrections from the perturbation theory. Therefore, in the high field limit, the three branches of excitations involving transitions from the lowest $|t, -\rangle$ state to the excited $|t, +\rangle$, $|t, 0\rangle$ and $|s\rangle$ levels should satisfy the following linear asymptotic behaviors:

$$\Delta E_1(B) = 2\mu_B g_J B \sqrt{(A_{\perp}^{(1)})^2 + (A_{\perp}^{(2)})^2} + O(1/B), \quad (33)$$

$$\Delta E_2(B) = \mu_B g_J B \sqrt{(A_{\perp}^{(1)})^2 + (A_{\perp}^{(2)})^2} + (E_{t,0}^{(1)} - E_{t,\pm}^{(1)}) + O(1/B), \quad (34)$$

$$\Delta E_3(B) = \mu_B g_J B \sqrt{(A_{\perp}^{(1)})^2 + (A_{\perp}^{(2)})^2} + (\epsilon_s - E_{t,\pm}^{(1)}) + O(1/B). \quad (35)$$

Due to the absence of symmetry-based selection rules, all the three branches are generally visible in the neutron scattering, terahertz spectroscopy or electron spin resonance experiments. By extrapolating the high-field behavior of the three excitations, we find that the branch 1 has twice the slope compared to the branch 2 and 3 with vanishing intercept along

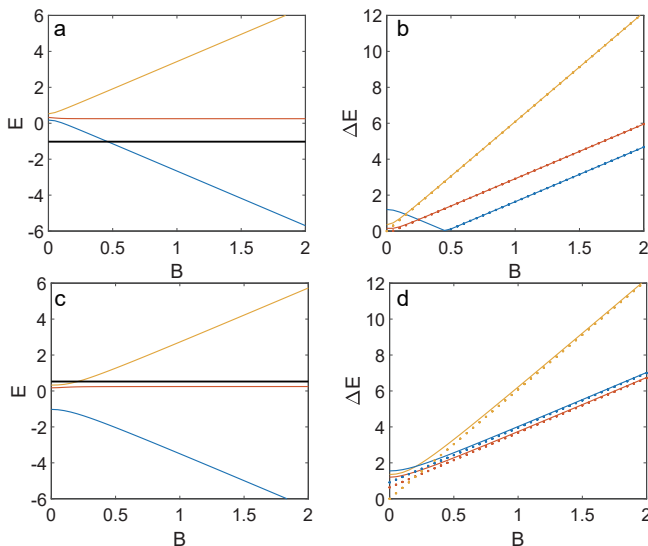


FIG. 7. **Evolution of energy spectra under external magnetic field** \parallel $[001]$. Energy levels and transition energies within **a,b** the singlet dimer phase, and **c,d** the triplet dimer phase. In **a,c** the singlet energy level is marked by the bold black line, while the three triplet levels are marked by colored solid lines. In **b,d** the high-field asymptotic behaviors of three excitations are indicated by dotted lines. The system parameters are identical to that in Fig. 6, except that the temperature T is set to zero.

the $B = 0$ axis. Meanwhile, branch 2 and 3 identical slopes with non-vanishing intercept along the $B = 0$ axis. From the evolution of energy spectrum under external magnetic fields, the experimental signatures of the singlet and triplet dimer phases are easily distinguishable:

- For the singlet dimer phase, the singlet level remains as the ground state at small fields, hence there must be a level crossing from singlet $|s\rangle$ to triplet $|t, -\rangle$ at a finite critical field B_c . This level crossing is expected to manifest as a non-analytical behavior of the excitation branch 3, where the gap closes and reopens across B_c , see Fig. 7**a,b**. A jump of magnetization across B_c is also expected;
- For the triplet dimer phase, the zero-field ground state is adiabatically connected to the high-field phase, meaning that a phase transition may not necessarily present. As a result, the gap-closing and reopening behavior observed in the singlet dimer phase is not expected. Instead, the excitation energies evolve smoothly with magnetic fields, exhibiting the high-field behaviors as discussed previously. See Fig. 7**c,d**.

IV. DISCUSSION AND CONCLUSION

In this work, we develop a theory describing the quantum magnetism of SS magnets with Kramers rare-earth ions. In contrast to the non-Kramers systems where the local

moments comprise both magnetic dipoles and quadrupoles, for Kramers systems all the effective-spin components are magnetic dipoles, with the dipole axes sublattice dependent. The interactions between local moments are described by an extended XYZ model on both intra- and inter-dimer bonds. For the dimer phase, we show that the exact solvability and nearly-localized triplet excitations within the dimer phase still remain valid in certain limit for the XYZ anisotropic model. We also show that a new “triplet” dimer phase can be stabilized by sufficiently strong exchange anisotropy, with more dispersive quantum excitations. We further illustrate the distinct behaviors of singlet and triplet dimer phases in response to external magnetic fields, as is summarized in Tab. I.

Here we discuss the issue of the antisymmetric DM interactions in this system. As the crystal structure does not have any inversion symmetry at each dimer bond center, for the pure spin system such as $RE=\text{Gd}$, spatial symmetry allows non-vanishing in-plane DM interactions within the dimer. However, for ordinary rare-earth magnets, the effective spins are made of the combination of spin and orbital angular momenta and subjected to strong SOC, hence transform differently under space group symmetries compared to pure spin systems. As a result, for both Kramers and non-Kramers systems, intra-dimer DM interaction is forbidden by the two mirror symmetries. Note that our result contrasts to a recent work on $\text{Er}_2\text{Be}_2\text{GeO}_7$ [57], where intra-dimer DM interactions explicitly breaking the four-fold S_4 symmetry were introduced. Nevertheless, within the framework of our theory, the inter-dimer DM interaction is still allowed given the absence of symmetry protection.

Then we discuss how to identify dimer phases in experiments. The phase diagram of the XYZ SS lattice model has been investigated in a similar context of non-Kramers systems [61], where the dimer, plaquette as well as antiferromagnetic phases have been identified. Different from plaquette and antiferromagnetic phases that break lattice translation or time-reversal symmetries, the dimer phase break no symmetry hence we expect no diverging behaviors in specific heat measurement upon cooling. Moreover, at low temperatures, the “singlet” and “triplet” dimer phases can be differentiated by their distinct behaviors upon external magnetic fields along the $[001]$ direction: The singlet dimer phase is stable against small fields, exhibiting a zero magnetization plateau with suppressed magnetic susceptibility at low temperatures. At large enough field, the singlet dimer state will be destroyed via level crossing, reflected by the gap closing and reopening behavior in the excitation spectra; In contrast, triplet dimer phases are more susceptible to the fields and do not form any zero magnetization plateau and exhibit pronounced low-temperature magnetic susceptibility. The excitation energies exhibit smooth behaviors with magnetic field due to absence of field-induced phase transition. In addition, more information about the exchange couplings can be inferred from their dynamical excitations. In the case of singlet dimers, inelastic neutron scattering generally reveals nearly-flat bands, where the band positions are directly

related to the intra-dimer exchange couplings, and that dispersions are influenced by the magnitude of specific off-diagonal inter-dimer interactions J^{13} , J^{23} , J^{31} and J^{32} . In contrast, triplet dimers show dispersion primarily influenced by diagonal inter-dimer interactions. Hence we can also estimate the strength of inter-dimer interactions by analyzing the bandwidth of excitations.

Finally, we discuss the implication of our results for the $\text{Yb}_2\text{Be}_2\text{GeO}_7$ compound [58, 60]. In this system, thermodynamic measurements reveal that magnetic entropy saturates to about $R \ln 2$ at around 3 K, indicating that each Yb^{3+} effectively behaves a spin-1/2 system with only the lowest Kramers doublet being relevant at low temperatures. Interestingly, no evidence of long-range magnetic order has been observed in either specific heat or susceptibility measurements down to 50 mK. Moreover, muon spin relaxation experiments reveal persistent spin dynamics down to 17 mK [60]. These experimental observations seem to suggest a quantum spin liquid ground state. However, the specific heat exhibits an activated behavior at sufficiently low temperatures, implying the presence of a finite gap of in this system. This gap is inconsistent with the characteristics of most spin liquid candidate materials but more indicative of a dimerized ground state. Furthermore, the nature of this dimerized phase can be identified with the published data: The magnetization curve along the [001] field direction at 0.4 K reveals the absence of a phase transition or zero-magnetization plateau, with quite pronounced magnetic susceptibilities at weak fields [58, 60]. Such behavior is rather inconsistent with a singlet dimer state but strongly suggests a triplet dimer ground state. This inference is further supported by the electron spin resonance (ESR) measurements, which show a smooth evolution of spectrum in all three excitation modes, indicating the absence of gap closure in the presence of magnetic field along \parallel [001]. In conclusion, all these comprehensive findings collectively suggest that $\text{Yb}_2\text{Be}_2\text{GeO}_7$ is more appropriately characterized as exhibiting a triplet dimer ground state.

METHODS

Bond-operator theory

We study the dispersion of excitations in the dimer phase using the Bond-operator method [67–69], a powerful tool that investigates the quantum dynamics of dimerized systems. In this formalism, each dimer state $|s\rangle$ or $|t_\alpha\rangle$ ($\alpha = 1, 2, 3$) can be expressed as applying bond-operator bosons \hat{s}^\dagger and \hat{t}_α^\dagger out of the vacuum $|\text{vac}\rangle$, *i.e.*,

$$|s\rangle = \hat{s}^\dagger |\text{vac}\rangle, |t_\alpha\rangle = \hat{t}_\alpha^\dagger |\text{vac}\rangle,$$

The Hilbert space of the bosons is larger than the original dimer Hilbert space and includes unphysical states. To limit the boson Hilbert space to its physical sector, a hard-core constraint must be imposed on each dimer,

$$\hat{s}^\dagger \hat{s} + \sum_\alpha \hat{t}_\alpha^\dagger \hat{t}_\alpha = 1. \quad (36)$$

The two spins within a dimer can be expressed as quadratics of bond operators,

$$\hat{\sigma}_1^\alpha = +\frac{1}{2} \left(\hat{s}^\dagger \hat{t}_\alpha + \hat{t}_\alpha^\dagger \hat{s} \right) - \frac{i}{2} \epsilon_{\alpha\beta\gamma} \hat{t}_\beta^\dagger \hat{t}_\gamma, \quad (37)$$

$$\hat{\sigma}_2^\alpha = -\frac{1}{2} \left(\hat{s}^\dagger \hat{t}_\alpha + \hat{t}_\alpha^\dagger \hat{s} \right) - \frac{i}{2} \epsilon_{\alpha\beta\gamma} \hat{t}_\beta^\dagger \hat{t}_\gamma, \quad (38)$$

Therefore we can rewrite the total Hamiltonian Eq. (4) in terms of bond-operators. The intra-dimer interaction H_J is diagonal in the bond-operator representation that can be recast as the chemical potential of bosons

$$H_J = \sum_{\mathbf{r}, \delta=A, B} \left(\epsilon_s \hat{s}_{\mathbf{r}, \delta}^\dagger \hat{s}_{\mathbf{r}, \delta} + \sum_\alpha \epsilon_t \hat{t}_{\mathbf{r}, \delta, \alpha}^\dagger \hat{t}_{\mathbf{r}, \delta, \alpha} \right), \quad (39)$$

while the inter-dimer H_J term are quartics of bond-operators that provides off-diagonal quantum dynamics to the system.

The elementary quantum excitations above the dimer ground states can be obtained by condensing the appropriate boson operators. Here we first take the singlet dimer state as an example, and the same strategy also applies to the triplet dimer states. In the singlet dimer state, the singlet operator \hat{s} is condensed

$$\hat{s} = \hat{s}^\dagger \approx \sqrt{1 - \sum_\alpha \hat{t}_\alpha^\dagger \hat{t}_\alpha}, \quad (40)$$

while the triplet operators \hat{t}_α can be regarded as elementary quantum excitations above the singlet dimer ground state.

Expanding the total Hamiltonian H in terms of \hat{t}_α up to the quadratic order and performing the Fourier transformation

$$\hat{s}_{\mathbf{r}, \delta} = \sqrt{\frac{2}{N}} \sum_{\mathbf{k} \in \text{BZ}} s_{\mathbf{k}, \delta} e^{i\mathbf{R}_\mathbf{r} \cdot \mathbf{k}}, \quad (41)$$

$$\hat{t}_{\mathbf{r}, \delta, \alpha} = \sqrt{\frac{2}{N}} \sum_{\mathbf{k} \in \text{BZ}} t_{\mathbf{k}, \delta, \alpha} e^{i\mathbf{R}_\mathbf{r} \cdot \mathbf{k}}, \quad (42)$$

at the quadratic order, we obtain the linear bond-operator Hamiltonian in a compact matrix form

$$H = \frac{1}{2} \sum_{\mathbf{k} \in \text{BZ}} \Psi(\mathbf{k})^\dagger \mathbf{M}(\mathbf{k}) \Psi(\mathbf{k}) + \text{const.} \quad (43)$$

where \mathbf{r} denotes the position of the unit cell, $\delta = A, B$ represents the dimer index within the unit cell, $\alpha = 1, 2, 3$, BZ denotes the Brillouin zone,

$$\Psi(\mathbf{k}) = [t_{\mathbf{k}, A, 1}, t_{\mathbf{k}, A, 2}, \dots, t_{\mathbf{k}, B, 3}, t_{-\mathbf{k}, A, 1}^\dagger, t_{-\mathbf{k}, A, 2}^\dagger, \dots, t_{-\mathbf{k}, B, 3}^\dagger]^T, \quad (44)$$

and $\mathbf{M}(\mathbf{k})$ is a 12×12 Hermitian matrix. Then we can Bogoliubov diagonalize H with $\Psi(\mathbf{k}) = T_{\mathbf{k}} \Phi(\mathbf{k})$, where

$$\Phi(\mathbf{k}) = [\beta_{\mathbf{k}, 1}, \beta_{\mathbf{k}, 2}, \dots, \beta_{\mathbf{k}, 6}, \beta_{-\mathbf{k}, 1}^\dagger, \beta_{-\mathbf{k}, 2}^\dagger, \dots, \beta_{-\mathbf{k}, 6}^\dagger]^T \quad (45)$$

is the diagonalized basis of Bogoliubov quasi-particles, and $T_{\mathbf{k}}$ is the transformation matrix. The diagonalized Hamiltonian reads

$$H = \frac{1}{2} \sum_{\mathbf{k} \in \text{BZ}} \Phi(\mathbf{k})^\dagger E(\mathbf{k}) \Phi(\mathbf{k}) + \text{const.}$$

$$= \sum_{\mathbf{k} \in \text{BZ}} \sum_{s=1}^6 \omega_{\mathbf{k}s} \beta_{\mathbf{k}s}^\dagger \beta_{\mathbf{k}s} + \text{const.}, \quad (46)$$

where $E(\mathbf{k}) = \text{diag}[\omega_{\mathbf{k}1}, \omega_{\mathbf{k}2}, \dots, \omega_{\mathbf{k}6}, \omega_{-\mathbf{k}1}, \omega_{-\mathbf{k}2}, \dots, \omega_{-\mathbf{k}6}]$ is the diagonalized Bogoliubov Hamiltonian.

Exact diagonalization

Deep in the dimer phases, the dimers are effectively decoupled, therefore it is save to ignore the inter-dimer interactions and consider independent dimers. Under the basis $\psi \equiv (|s\rangle |t_1\rangle |t_2\rangle |t_3\rangle)^T$, the Hamiltonian for each dimer can be represented by 4×4 matrices. By diagonalizing such Hamiltonians, physical quantities such as energies and magnetizations can be obtained.

DATA AVAILABILITY

The data that support the findings of this study are available from the corresponding authors upon reasonable request.

CODE AVAILABILITY

The code that supports the findings of this study is available from the corresponding authors upon reasonable request.

ACKNOWLEDGMENTS

We thank H. Zhou, X. Sun and J. Ma for useful discussions. This work is supported by the National Key R&D Program of China (Grant No.2023YFA1406500), and the National Science Foundation of China (Grant Nos.12334008 and 12174441).

AUTHOR CONTRIBUTIONS

The project was conceived by R.Y. and C.L.. Symmetry analysis was performed by C.L.. Bond-operator calculation was performed by C.L. and G.D.. Magnetization calculations were performed by G.D.. Theoretical interpretation was provided by R.Y., C.L., G.D.. The manuscript was written by C.L. and R.Y. with contributions from all the authors.

COMPETING INTERESTS

The authors declare no competing interests.

-
- [1] B. S. Shastry and B. Sutherland, Exact ground state of a quantum mechanical antiferromagnet, *Physica B+C* **108**, 1069 (1981).
- [2] S. Miyahara and K. Ueda, Exact dimer ground state of the two dimensional Heisenberg spin system $\text{SrCu}_2(\text{BO}_3)_2$, *Phys. Rev. Lett.* **82**, 3701 (1999).
- [3] H. Kageyama, K. Yoshimura, R. Stern, N. Mushnikov, K. Onizuka, M. Kato, K. Kosuge, C. Slichter, T. Goto, and Y. Ueda, Exact dimer ground state and quantized magnetization plateaus in the two-dimensional spin system $\text{SrCu}_2(\text{BO}_3)_2$, *Phys. Rev. Lett.* **82**, 3168 (1999).
- [4] A. Koga and N. Kawakami, Quantum phase transitions in the Shastry-Sutherland model for $\text{SrCu}_2(\text{BO}_3)_2$, *Phys. Rev. Lett.* **84**, 4461 (2000).
- [5] P. A. McClarty, F. Krüger, T. Guidi, S. Parker, K. Refson, *et al.*, Topological triplon modes and bound states in a Shastry–Sutherland magnet, *Nat. Phys.* **13**, 736 (2017).
- [6] M. Song, K. Cho, J. Lee, and B. Cho, Abnormal field-dependence of magnetocaloric effect in ErB_4 and TmB_4 , *AIP Adv.* **10** (2020).
- [7] J. Guo, G. Sun, B. Zhao, L. Wang, W. Hong, *et al.*, Quantum phases of $\text{SrCu}_2(\text{BO}_3)_2$ from high-pressure thermodynamics, *Phys. Rev. Lett.* **124**, 206602 (2020).
- [8] Y. Cui, L. Liu, H. Lin, K.-H. Wu, W. Hong, *et al.*, Proximate deconfined quantum critical point in $\text{SrCu}_2(\text{BO}_3)_2$, *Science* **380**, 1179 (2023).
- [9] T. Nomura, P. Corboz, A. Miyata, S. Zherlitsyn, Y. Ishii, *et al.*, Unveiling new quantum phases in the Shastry-Sutherland compound $\text{SrCu}_2(\text{BO}_3)_2$ up to the saturation magnetic field, *Nat. Commun.* **14**, 3769 (2023).
- [10] S. Miyahara and K. Ueda, Theory of the orthogonal dimer Heisenberg spin model for $\text{SrCu}_2(\text{BO}_3)_2$, *J. Phys. Condens. Matter* **15**, R327 (2003).
- [11] M. Zayed, C. Rüegg, J. Larrea J, A. Läuchli, Panagopoulos, *et al.*, 4-spin plaquette singlet state in the Shastry–Sutherland compound $\text{SrCu}_2(\text{BO}_3)_2$, *Nat. Phys.* **13**, 962 (2017).
- [12] E. Müller-Hartmann, R. R. Singh, C. Knetter, and G. S. Uhrig, Exact demonstration of magnetization plateaus and first-order dimer-Néel phase transitions in a modified Shastry-Sutherland model for $\text{SrCu}_2(\text{BO}_3)_2$, *Phys. Rev. Lett.* **84**, 1808 (2000).
- [13] K. Onizuka, H. Kageyama, Y. Narumi, K. Kindo, Y. Ueda, *et al.*, 1/3 magnetization plateau in $\text{SrCu}_2(\text{BO}_3)_2$ -stripe order of excited triplets, *J. Phys. Soc. Jpn.* **69**, 1016 (2000).
- [14] M. Takigawa, K. Kodama, M. Horvatić, C. Berthier, H. Kageyama, *et al.*, The 1/8-magnetization plateau state in the 2D quantum antiferromagnet $\text{SrCu}_2(\text{BO}_3)_2$: spin superstructure, phase transition, and spin dynamics studied by high-field NMR, *Physica B* **346**, 27 (2004).
- [15] F. Levy, I. Sheikin, C. Berthier, M. Horvatić, M. Takigawa, H. Kageyama, T. Waki, and Y. Ueda, Field dependence of the quantum ground state in the Shastry-Sutherland system $\text{SrCu}_2(\text{BO}_3)_2$, *Europhys. Lett.* **81**, 67004 (2008).

- [16] M. Jaime, R. Daou, S. A. Crooker, F. Weickert, A. Uchida, A. E. Feiguin, C. D. Batista, H. A. Dabkowska, and B. D. Gaulin, Magnetostriction and magnetic texture to 100.75 tesla in frustrated $\text{SrCu}_2(\text{BO}_3)_2$, *Proc. Natl. Acad. Sci.* **109**, 12404 (2012).
- [17] J. Wang, H. Li, N. Xi, Y. Gao, Q.-B. Yan, W. Li, and G. Su, Plaquette singlet transition, magnetic barocaloric effect, and spin supersolidity in the Shastry-Sutherland model, *Phys. Rev. Lett.* **131**, 116702 (2023).
- [18] J. L. Jiménez, S. P. Crone, E. Fogh, M. E. Zayed, R. Lortz, E. Pomjakushina, K. Conder, A. M. Läuchli, L. Weber, S. Wessel, *et al.*, A quantum magnetic analogue to the critical point of water, *Nature* **592**, 370 (2021).
- [19] Y. Cui, K. Du, Z. Wu, S. Li, P. Yang, Y. Chen, X. Xu, H. Chen, C. Li, J. Liu, *et al.*, Two plaquette-singlet phases in the shastry-sutherland compound $\text{SrCu}_2(\text{BO}_3)_2$, arXiv preprint arXiv:2411.00302 (2024).
- [20] S. Haravifard, B. Gaulin, Z. Yamani, S. Dunsiger, and H. Dabkowska, Neutron scattering from the static and dynamic lattice of $\text{SrCu}_2(\text{BO}_3)_2$ in its Shastry-Sutherland singlet ground state, *Phys. Rev. B* **85**, 134104 (2012).
- [21] M. Zayed, C. Rüegg, T. Strässle, U. Stuhr, B. Roessli, M. Ay, J. Mesot, P. Link, E. Pomjakushina, M. Stingaciu, *et al.*, Correlated decay of triplet excitations in the Shastry-Sutherland compound $\text{SrCu}_2(\text{BO}_3)_2$, *Phys. Rev. Lett.* **113**, 067201 (2014).
- [22] J. Y. Lee, Y.-Z. You, S. Sachdev, and A. Vishwanath, Signatures of a deconfined phase transition on the Shastry-Sutherland lattice: Applications to quantum critical $\text{SrCu}_2(\text{BO}_3)_2$, *Phys. Rev. X* **9**, 041037 (2019).
- [23] N. Xi, H. Chen, Z. Xie, and R. Yu, Plaquette valence bond solid to antiferromagnet transition and deconfined quantum critical point of the Shastry-Sutherland model, *Phys. Rev. B* **107**, L220408 (2023).
- [24] P. Corboz and F. Mila, Tensor network study of the Shastry-Sutherland model in zero magnetic field, *Phys. Rev. B* **87**, 115144 (2013).
- [25] J. Yang, A. W. Sandvik, and L. Wang, Quantum criticality and spin liquid phase in the Shastry-Sutherland model, *Phys. Rev. B* **105**, L060409 (2022).
- [26] H. Chen, G. Duan, C. Liu, Y. Cui, W. Yu, Z. Xie, and R. Yu, Spin excitations of the shastry-sutherland model—altermagnetism and proximate deconfined quantum criticality, arXiv preprint arXiv:2411.00301 (2024).
- [27] L. Balents, Spin liquids in frustrated magnets, *Nature* **464**, 199 (2010).
- [28] L. Savary and L. Balents, Quantum spin liquids: a review, *Rep. Prog. Phys.* **80**, 016502 (2016).
- [29] Y. Zhou, K. Kanoda, and T.-K. Ng, Quantum spin liquid states, *Rev. Mod. Phys.* **89**, 025003 (2017).
- [30] C. Broholm, R. Cava, S. Kivelson, D. Nocera, M. Norman, and T. Senthil, Quantum spin liquids, *Science* **367**, eaay0668 (2020).
- [31] H.-S. Kim, V. S. V. A. Catuneanu, and H.-Y. Kee, Kitaev magnetism in honeycomb RuCl_3 with intermediate spin-orbit coupling, *Phys. Rev. B* **91**, 241110 (2015).
- [32] S.-H. Baek, S.-H. Do, K.-Y. Choi, Y. S. Kwon, A. Wolter, S. Nishimoto, J. Van Den Brink, and B. Büchner, Evidence for a field-induced quantum spin liquid in $\alpha\text{-RuCl}_3$, *Phys. Rev. Lett.* **119**, 037201 (2017).
- [33] T. Takayama, A. Kato, R. Dinnebier, J. Nuss, H. Kono, L. Veiga, G. Fabbris, D. Haskel, and H. Takagi, Hyperhoneycomb iridate $\beta\text{-Li}_2\text{IrO}_3$ as a platform for Kitaev magnetism, *Phys. Rev. Lett.* **114**, 077202 (2015).
- [34] I. Rousochatzakis, N. B. Perkins, Q. Luo, and H.-Y. Kee, Beyond Kitaev physics in strong spin-orbit coupled magnets, *Rep. Prog. Phys.* **87**, 026502 (2024).
- [35] Z. Zhang, Y. Cai, J. Kang, Z. Ouyang, Z. Zhang, A. Zhang, J. Ji, F. Jin, and Q. Zhang, Anisotropic exchange coupling and ground state phase diagram of Kitaev compound YbOCl , *Phys. Rev. Research* **4**, 033006 (2022).
- [36] A. Liu, F. Song, H. Bu, Z. Li, M. Ashtar, Y. Qin, D. Liu, Z. Xia, J. Li, Z. Zhang, *et al.*, $\text{Ba}_9\text{RE}_2(\text{SiO}_4)_6$ (RE= Ho–Yb): A family of rare-earth-based honeycomb-lattice magnets, *Inorg. Chem.* **62**, 13867 (2023).
- [37] S.-H. Jang, R. Sano, Y. Kato, and Y. Motome, Antiferromagnetic kitaev interaction in f -electron based honeycomb magnets, *Phys. Rev. B* **99**, 241106 (2019).
- [38] S.-H. Jang, R. Sano, Y. Kato, and Y. Motome, Computational design of f -electron kitaev magnets: Honeycomb and hyperhoneycomb compounds $A_2\text{pro}_3$ (a = alkali metals), *Phys. Rev. Mater.* **4**, 104420 (2020).
- [39] J. G. Rau and M. J. Gingras, Frustrated quantum rare-earth pyrochlores, *Annu. Rev. Condens. Matter Phys.* **10**, 357 (2019).
- [40] E. M. Smith, J. Dudemaine, B. Placke, R. Schäfer, D. R. Yahne, T. DeLazzer, A. Fitterman, J. Beare, J. Gaudet, C. R. Buhariwalla, *et al.*, Quantum spin ice response to a magnetic field in the dipole-octupole pyrochlore $\text{Ce}_2\text{Zr}_2\text{O}_7$, *Phys. Rev. B* **108**, 054438 (2023).
- [41] A. M. Hallas, J. Gaudet, and B. D. Gaulin, Experimental insights into ground-state selection of quantum XY pyrochlores, *Annu. Rev. Condens. Ma. P.* **9**, 105 (2018).
- [42] Y.-D. Li, Y. Shen, Y. Li, J. Zhao, and G. Chen, Effect of spin-orbit coupling on the effective-spin correlation in YbMgGaO_4 , *Phys. Rev. B* **97**, 125105 (2018).
- [43] J. A. Paddison, M. Daum, Z. Dun, G. Ehlers, Y. Liu, M. B. Stone, H. Zhou, and M. Mourigal, Continuous excitations of the triangular-lattice quantum spin liquid YbMgGaO_4 , *Nat. Phys.* **13**, 117 (2017).
- [44] Y. Shen, Y.-D. Li, H. Wo, Y. Li, S. Shen, B. Pan, Q. Wang, H. Walker, P. Steffens, M. Boehm, *et al.*, Evidence for a spinon Fermi surface in a triangular-lattice quantum-spin-liquid candidate, *Nature* **540**, 559 (2016).
- [45] M. M. Bordelon, E. Kenney, C. Liu, T. Hogan, L. Posthuma, M. Kavand, Y. Lyu, M. Sherwin, N. P. Butch, C. Brown, *et al.*, Field-tunable quantum disordered ground state in the triangular-lattice antiferromagnet NaYbO_2 , *Nat. Phys.* **15**, 1058 (2019).
- [46] Y. Li, G. Chen, W. Tong, L. Pi, J. Liu, Z. Yang, X. Wang, and Q. Zhang, Rare-earth triangular lattice spin liquid: a single-crystal study of YbMgGaO_4 , *Phys. Rev. Lett.* **115**, 167203 (2015).
- [47] B. Gao, T. Chen, C. Liu, M. L. Klemm, S. Zhang, Z. Ma, X. Xu, C. Won, G. T. McCandless, N. Murai, *et al.*, Spin excitation continuum in the exactly solvable triangular-lattice spin liquid $\text{CeMgAl}_{11}\text{O}_{19}$, arXiv preprint arXiv:2408.15957 (2024).
- [48] Z. Ma, J. Wang, Z.-Y. Dong, J. Zhang, S. Li, S.-H. Zheng, Y. Yu, W. Wang, L. Che, K. Ran, *et al.*, Spin-glass ground state in a triangular-lattice compound YbZnGaO_4 , *Phys. Rev. Lett.* **120**, 087201 (2018).
- [49] I. Kimchi, A. Nahum, and T. Senthil, Valence bonds in random quantum magnets: theory and application to YbMgGaO_4 , *Phys. Rev. B* **8**, 031028 (2018).
- [50] T. Xie, A. Eberharter, J. Xing, S. Nishimoto, M. Brando, P. Khanenko, J. Sichelschmidt, A. Turrini, D. Mazzone, P. Naumov, *et al.*, Complete field-induced spectral response of the spin-1/2 triangular-lattice antiferromagnet CsYbSe_2 , *npj Quantum Mater* **8**, 48 (2023).

- [51] M. Ashtar, Y. Gao, C. Wang, Y. Qiu, W. Tong, Y. Zou, X. Zhang, M. Marwat, S. Yuan, and Z. Tian, Synthesis, structure and magnetic properties of rare-earth $\text{REMgAl}_{11}\text{O}_{19}$ (RE= Pr, Nd) compounds with two-dimensional triangular lattice, *J. Alloy. Compd.* **802**, 146 (2019).
- [52] N. Li, A. Brassington, M. Shu, Y. Wang, H. Liang, Q. Li, X. Zhao, P. Baker, H. Kikuchi, T. Masuda, *et al.*, Spinons in a new Shastry-Sutherland lattice magnet $\text{Pr}_2\text{Ga}_2\text{BeO}_7$, arXiv preprint arXiv:2405.13628 (2024).
- [53] A. Brassington, Q. Ma, G. Sala, A. I. Kolesnikov, K. M. Taddei, Y. Wu, E. S. Choi, H. Wang, W. Xie, J. Ma, H. D. Zhou, and A. A. Aczel, Magnetic properties of the quasi-XY Shastry-Sutherland magnet $\text{Er}_2\text{Be}_2\text{SiO}_7$, *Phys. Rev. Mater.* **8**, 094001 (2024).
- [54] A. Brassington, Q. Huang, A. Aczel, and H. Zhou, Synthesis and magnetic properties of the Shastry-Sutherland family $\text{R}_2\text{Be}_2\text{SiO}_7$ (R= Nd, Sm, Gd-Yb), *Phys. Rev. Mater.* **8**, 014005 (2024).
- [55] A. Liu, F. Song, Y. Cao, H. Ge, H. Bu, J. Zhou, Y. Qin, Q. Zeng, J. Li, L. Ling, *et al.*, Distinct magnetic ground states in Shastry-Sutherland lattice materials: $\text{Pr}_2\text{Be}_2\text{GeO}_7$ versus $\text{Nd}_2\text{Be}_2\text{GeO}_7$, *Phys. Rev. B.* **109**, 184413 (2024).
- [56] Y. Ishii, G. Sala, M. B. Stone, V. O. Garlea, S. Calder, J. Chen, H. K. Yoshida, S. Fukuoka, J. Yan, C. dela Cruz, *et al.*, Magnetic properties of the Shastry-Sutherland lattice material $\text{BaNd}_2\text{ZnO}_5$, *Phys. Rev. Mater.* **5**, 064418 (2021).
- [57] L. Yadav, A. Rufino, R. Bag, A. I. Kolesnikov, V. O. Garlea, D. Graf, F. Mila, S. Haravifard, *et al.*, Observation of unprecedented fractional magnetization plateaus in a new Shastry-Sutherland Ising compound, arXiv preprint arXiv:2405.12405 (2024).
- [58] A. Liu, J. Zhou, L. Wang, Y. Cao, F. Song, Y. Han, J. Li, W. Tong, Z. Xia, Z. Ouyang, J. Zhao, H. Guo, and Z. Tian, Large magnetocaloric effect in the Shastry-Sutherland lattice compound $\text{Yb}_2\text{Be}_2\text{GeO}_7$ with spin-disordered ground state, *Phys. Rev. B* **110**, 144445 (2024).
- [59] M. Ashtar, Y. Bai, L. Xu, Z. Wan, Z. Wei, Y. Liu, M. A. Marwat, and Z. Tian, Structure and magnetic properties of melilite-type compounds $\text{RE}_2\text{Be}_2\text{GeO}_7$ (RE= Pr, Nd, Gd-Yb) with rare-earth ions on Shastry-Sutherland lattice, *Inorg. Chem.* **60**, 3626 (2021).
- [60] M. Pula, S. Sharma, J. Gautreau, S. KP, A. Kanigel, M. Frontzek, T. Dolling, L. Clark, S. Dunsiger, A. Ghara, *et al.*, Candidate for a quantum spin liquid ground state in the Shastry-Sutherland lattice material $\text{Yb}_2\text{Be}_2\text{GeO}_7$, *Phys. Rev. B.* **110**, 014412 (2024).
- [61] G. Duan, R. Yu, and C. Liu, Theory of magnetism for rare-earth magnets on the shastry-sutherland lattice with non-kramers ions, *Phys. Rev. B* **110**, 214410 (2024).
- [62] M. Pula, S. Sharma, J. Gautreau, A. Kanigel, C. Cruz, T. Dolling, L. Clark, G. Luke, *et al.*, Fractionalized magnetization plateaus in the Shastry-Sutherland lattice material $\text{Er}_2\text{Be}_2\text{GeO}_7$, arXiv preprint arXiv:2412.04360 (2024).
- [63] I. Dzyaloshinsky, A thermodynamic theory of “weak” ferromagnetism of antiferromagnetics, *J. Phys. Chem. Solids* **4**, 241 (1958).
- [64] T. Moriya, Anisotropic superexchange interaction and weak ferromagnetism, *Phys. Rev.* **120**, 91 (1960).
- [65] S. Miyahara and K. Ueda, Superstructures at magnetization plateaus in $\text{SrCu}_2(\text{BO}_3)_2$, *Phys. Rev. B.* **61**, 3417 (2000).
- [66] H. Kageyama, M. Nishi, N. Aso, K. Onizuka, T. Yoshihama, K. Nukui, K. Kodama, K. Kakurai, and Y. Ueda, Direct evidence for the localized single-triplet excitations and the dispersive multitriplet excitations in $\text{SrCu}_2(\text{BO}_3)_2$, *Phys. Rev. Lett.* **84**, 5876 (2000).
- [67] A. Läuchli, S. Wessel, and M. Sigrist, Phase diagram of the quadrumerized Shastry-Sutherland model, *Phys. Rev. B.* **66**, 014401 (2002).
- [68] P. McClarty, X.-Y. Dong, M. Gohlke, J. Rau, F. Pollmann, *et al.*, Topological magnons in Kitaev magnets at high fields, *Phys. Rev. B.* **98**, 060404 (2018).
- [69] S. Sachdev and R. Bhatt, Bond-operator representation of quantum spins: Mean-field theory of frustrated quantum Heisenberg antiferromagnets, *Phys. Rev. B.* **41**, 9323 (1990).
- [70] C. Knetter, A. Bühler, E. Müller-Hartmann, and G. S. Uhrig, Dispersion and symmetry of bound states in the Shastry-Sutherland model, *Phys. Rev. Lett.* **85**, 3958 (2000).
- [71] C. Knetter, E. Müller-Hartmann, and G. S. Uhrig, Symmetries and triplet dispersion in a modified Shastry-Sutherland model for $\text{SrCu}_2(\text{BO}_3)_2$, *J. Phys. Condens. Matter* **12**, 9069 (2000).